24th INTERNATIONAL CONGRESS ON SOUND AND VIBRATION
23–27 July 2017, London

ICSV24
23-27JULY 2017
LONDON CALLING

STABILITY ANALYSIS OF A MATRIX BURNER FLAME USING A GENERALISED HEAT RELEASE RATE LAW FEATURING MULTIPLE TIME-LAGS

Sreenath Malamal Gopinathan and Maria A. Heckl
Keele University, School of Chemical and Physical Sciences, Staffordshire, ST55BG, UK
email: s.malamal.gopinathan@keele.ac.uk

In the present work, we perform a stability analysis of a matrix burner configuration consisting of a semi-infinite 1D duct. It is closed with a rigid piston at the upstream end. A cavity is formed by a perforated plate placed a finite distance downstream of the piston; this perforated plate also acts as a flame holder, in that it stabilises a matrix flame. The distance between the closed end and the perforated plate, i.e. the cavity length, can be varied by varying the piston location. Our model for the flame is based on the Flame Describing Function (amplitude-dependent flame transfer function) measured by Noiray (Ph.D. Thesis, École Centrale Paris, 2007). It is an analytical expression and features two prominent time-lags, i.e. we write the heat release rate in terms of the time-delayed velocity as a superposition of two Gaussians, each characterised by three amplitude-dependent quantities: central time-lag, peak value and standard deviation. The parameters of our time-lag model are deduced from the experimental Flame Describing Function using error minimisation and nonlinear optimisation techniques. We then analyse the stability behaviour of the combustion system using a tailored Green's function approach. The main parameters of interest are the amplitude and the cavity length.

Keywords: burner, multiple time-lags, Green's function, stability analysis

1. Introduction

In combustion systems like gas turbine engines, feedback between pressure oscillations and the resulting heat release rate fluctuations can cause high-amplitude oscillations, which are called thermoacoustic instabilities. They can cause severe structural/hardware damage.

An important feature of models to predict such instabilities is the heat release law, i.e. the relationship between the rate of heat released by the flame and the acoustic velocity that perturbs the flame. This relationship can be measured (by exciting an acoustic field and measuring the resulting fluctuations in the heat release rate). Fourier transform of the measured time histories gives the Flame Transfer Function (FTF). This is a frequency-domain quantity, defined by

$$\mathcal{T}(\omega) = \frac{\hat{Q}(\omega)/\bar{Q}}{\hat{u}(\omega)/\bar{u}}, \tag{1}$$

where $\hat{Q}(\omega)$ is the rate of heat release and $\hat{u}(\omega)$ is the acoustic velocity, and $\bar{Q}$, $\bar{u}$ are the corresponding mean values.

Typically, a measured FTF is available at certain frequency values in a given frequency range. If this is to be used in low-order models, it needs to be converted into an analytical expression. Early attempts to obtain such an expression have been made by Heckl [1, 2]; she constructed a heat release

law from FTF values measured by Noiray [3] for a matrix burner. This was effectively an extended $n\tau$- law, containing not only a time-delayed velocity term, but also an instantaneous term. Furthermore, the time-lag and coupling coefficients were dependent on the excitation amplitude, and she also represented this amplitude dependence analytically, based on Noiray's measurements at different amplitudes. This allowed the study of the stability behaviour of the matrix burner, using a tailored Green's function method.

In this paper, we follow the method described in [1, 2], but analytically represent the FTF and its amplitude-dependence in a more general and systematic way. The new heat release law will be described in terms of a multiple time-lag distribution, both in the time and frequency domain. This is shown in section 2. The tailored Green's function approach and stability calculations are outlined in section 3. Stability predictions are given in section 4, followed by the discussions and outlook.

2. Multiple time-lag (MTL) approximation

The dynamic behaviour of many flames is characterised by two or more prominent time-lags, and by a distribution of the heat release rate around these time-lags. Let us assume a generic heat release rate law with k prominent time-lags $\tau_1,\ \tau_2,\ \cdots,\ \tau_k$, and with a Gaussian distribution D centred around each of them,

$$\frac{Q^{'}(t)}{\bar{Q}} = n_1 \int_{-\infty}^{\infty} \frac{u^{'}(t-\tau)}{\bar{u}} D(\tau-\tau_1)d\tau + n_2 \int_{-\infty}^{\infty} \frac{u^{'}(t-\tau)}{\bar{u}} D(\tau-\tau_2)d\tau + \cdots + n_k \int_{-\infty}^{\infty} \frac{u^{'}(t-\tau)}{\bar{u}} D(\tau-\tau_k)d\tau, \tag{2}$$

where D, is given by

$$D(\tau-\tau_j) = \frac{1}{\sigma_j\sqrt{2\pi}}\, e^{\left(\frac{-(\tau-\tau_j)^2}{2\sigma_j^2}\right)}, \quad j = 1,\ 2,\ \cdots,\ k. \tag{3}$$

Eq. (2) contains $3k$ parameters, $\tau_1,\ \tau_2,\ \cdots,\ \tau_k, n_1,\ n_2,\ \cdots,\ n_k$ and $\sigma_1,\ \sigma_2,\ \cdots,\ \sigma_k$, which are treated as fitting parameters and assumed to be amplitude-dependent. Taking the Fourier transform of Eq. (2). and rearranging, we get the FTF for each amplitude of excitation, i.e. the Flame Describing Function (FDF) as

$$\begin{aligned}\mathcal{T}_k(A,\omega) &= \frac{\hat{Q}(\omega,A)/\bar{Q}}{\hat{u}(\omega,A)/\bar{u}} \\ &= n_1(A)e^{\frac{-\omega^2\sigma_1(A)^2}{2}}e^{i\omega\tau_1(A)} + n_2(A)e^{\frac{-\omega^2\sigma_2(A)^2}{2}}e^{i\omega\tau_2(A)} + \cdots + n_k(A)e^{\frac{-\omega^2\sigma_k(A)^2}{2}}e^{i\omega\tau_k(A)}.\end{aligned} \tag{4}$$

The unknown fitting parameters in this multiple time-lag approximation are determined using by the optimisation routine `fminsearch` in MATLAB® and minimising the error between approximated FDF and the actual FDF for all amplitudes of excitation at which measurement data are available. We also impose the additional constraint that $|\mathcal{T}_K(A,\omega)| = 1$ at $\omega = 0$, which gives

$$\sum_{j=1}^{k} n_j = 1. \tag{5}$$

The amplitude dependence of each parameter in the MTL approximation is also modelled analytically by representing it by a linear function, Altogether, we obtain a fully analytical expression for the FDF.

We now apply the multiple time-lag expression (Eq. 4) to approximate the FDF measured by Noiray [3, 4]. This has only two prominent time-lags [5], so only two terms need to be included,

$$\mathcal{T}_2(A,\omega) = n_1(A)e^{\frac{-\omega^2\sigma_1(A)^2}{2}}e^{i\omega\tau_1(A)} + n_2(A)e^{\frac{-\omega^2\sigma_2(A)^2}{2}}e^{i\omega\tau_2(A)}, \tag{6}$$

and Eq. (5) reduces to

$$n_1 + n_2 = 1. \tag{7}$$

The unknowns are n_1, n_2, τ_1, τ_2, σ_1 and σ_2. Experimental FDF data are available for 5 amplitude values: $A/\bar{u} = 0.13, 0.23, 0.40, 0.48,$ and 0.54. The optimum values of n_1, n_2, τ_1, τ_2, σ_1 and σ_2 were calculated with the MATLAB® routine `fminsearch` individually for each amplitude. The results are shown by symbols in Fig. 1. It is evident that they depend on amplitude. We model this amplitude dependence by a linear function. This is shown by the dashed lines in Fig. 1: the lines for n_1, τ_1, τ_2, and σ_1 have a positive slope, and those for n_2, and σ_2 have a negative slope. Numerical values for the slope and the vertical position of each line were obtained by least squares method; (disregarding the results for $A/\bar{u} = 0.54$, which seem to be outliers); they are listed in Table 1.

Eq. (6), together with the parameters listed in Table 1, represents a fully analytical approximation of the measured FDF. It also gives us an extrapolation for higher amplitude values for which experimental data are not available.

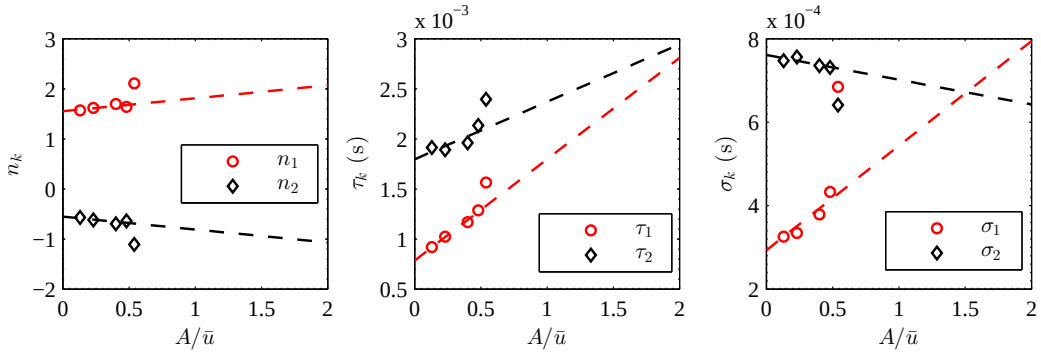

Figure 1: Amplitude dependence of the model parameters for the FDF approximated with the two time-lag model. The dashed lines represent linear approximations for the amplitude dependence. The amplitude dependence is tabulated in Table 1.

Table 1: Amplitude dependence of the model parameters approximated by linear functions.

Parameter	Dependence on $A/\bar{u}$
n_1	$0.25877(A/\bar{u}) + 1.5515$
n_2	$-0.25873(A/\bar{u}) - 0.55153$
τ_1	$0.0010114(A/\bar{u}) + 0.00078563$
τ_2	$0.00057397(A/\bar{u}) + 0.0017958$
σ_1	$0.00025061(A/\bar{u}) + 0.00029299$
σ_2	$-5.9323\times10^{-05}(A/\bar{u}) + 0.00076098$

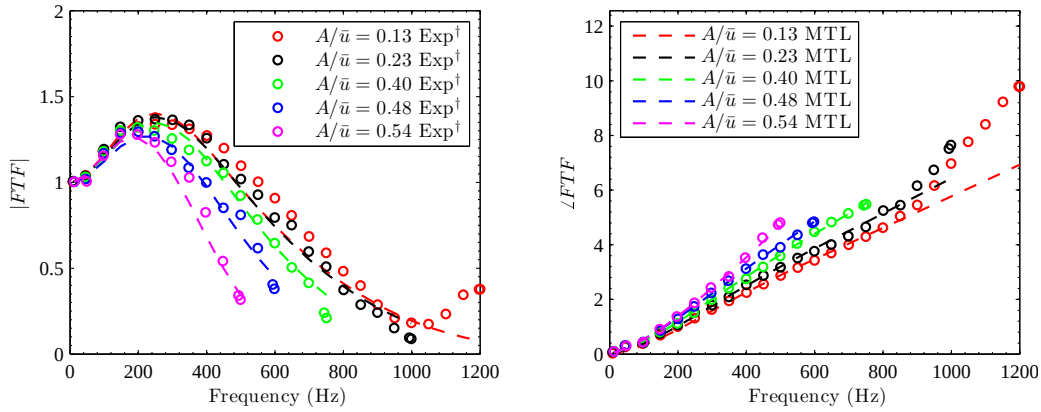

Figure 2: Gain (left) and Phase (right) vs frequency for the FDF of a matrix burner flame. Markers: experimental values; continuous curves: analytical approximations using the expressions given in Table 1.

Figure 2 shows the measured FDF with markers, and the MTL approximation with continuous curves. It is observed that that measured values and the MTL approximation have good agreement.

3. Stability Analysis

3.1 Matrix Burner

A schematic picture of the matrix burner used in Noiray's work is given in Fig. 3. The setup consists of a circular tube with a piston (variable position) at one end and a perforated plate at the other end. The perforated plate acts as the flame holder and gives a matrix of flames.

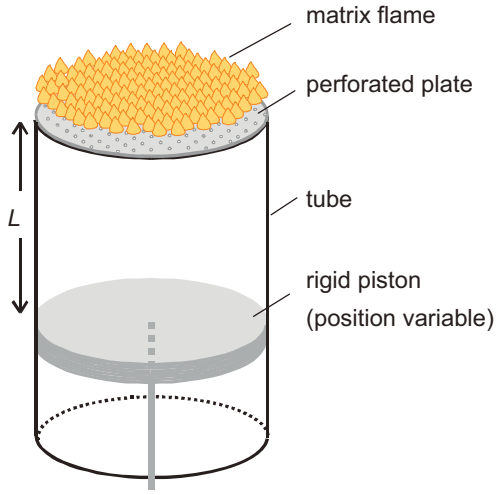

Figure 3: Schematic of Noiray's matrix burner.

In order to model this set-up analytically, we make the following assumptions.

1. The sound field is purely 1-D, not only inside the tube, but also beyond its downstream end. The wave transmitted beyond this end is of course 3-D, but we ignore this and instead assume that the tube has a semi-infinite continuation, which keeps the transmitted wave 1-D.
2. We model the perforated plate at the otherwise open end as a pair of two interfaces at $x = L$ and $x = L + \Delta$, respectively, each with a given transmission and reflection coefficient; the distance Δ between them is very small, $\Delta \to 0$.
3. The upstream end is modelled as rigid with a reflection coefficient of $R_0 = 1$.
4. The mean temperature and speed of sound (denoted by c) are uniform throughout the semi-infinite tube.

The modelled configuration is shown in Fig. 4. The tube is divided into 3 regions, A, B and C, separated by the interfaces at $x = L$ (perforated plate) and $x = L + \Delta$ (open end). Acoustic waves travel backward and forward with wave number $k = \omega/c$. a_+, b_+, c_+ are pressure amplitudes of the waves travelling in the positive direction, and a_-, b_- of those travelling in the negative direction. The

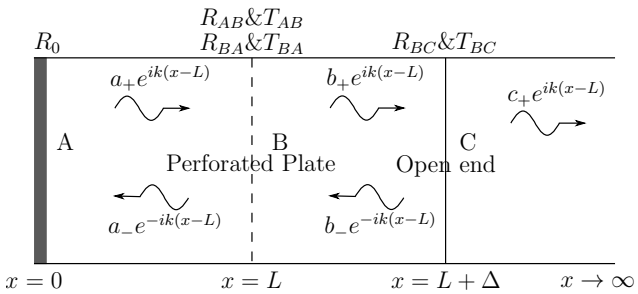

Figure 4: The modelled configuration, showing the acoustic waves and reflection and transmission coefficients.

reflection and transmission coefficients of the perforated plate are given by

$$R_{AB} = \frac{\omega}{\omega + 2i\mathcal{N}cK} \text{ and } T_{AB} = \frac{2i\mathcal{N}cK}{\omega + 2i\mathcal{N}cK}, \tag{8a, 8b}$$

where $\mathcal{N}$ is the number of holes per unit area, c is the speed of sound, and K is the Rayleigh conductivity. For a plate of thickness h and with circular holes of radius r_p,

$$K = \frac{r_p^2 \pi}{r_p \pi/2 + h}. \tag{9}$$

For symmetry reasons we have $R_{BA} = R_{AB}$ & $T_{BA} = T_{AB}$ for waves coming from the other direction (i.e. going from region B to region A). The reflection coefficient of an unflanged open tube end of radius a is known from [6],

$$R_{BC} = -\frac{1 - [(1/4)(\omega a/c^2) - i(\omega a/c)0.6133]}{1 + [(1/4)(\omega a/c^2) - i(\omega a/c)0.6133]}. \tag{10}$$

The corresponding transmission coefficient T_{BC} is given by (see [1])

$$T_{BC} = |T_{BC}|\, e^{i\varphi}, \text{ with } |T_{BC}| = \sqrt{1 - |R_{BC}|^2} \text{ and } \varphi = Arg(1 - R_{BC}). \tag{11}$$

Also, we have $R_{BC} = R_{CB}$ & $T_{BC} = T_{CB}$ for the waves hitting the interface between regions B and C from the right.

The reflection and transmission coefficient of the combined interface of perforated plate and open end has been calculated in [1], and these results for $\Delta \to 0$ are

$$R_{AC} = \frac{R_{AB} - R_{AB}R_{BA}R_{BC} + T_{AB}T_{BA}T_{BC}}{1 - R_{BA}R_{BC}} \text{ and } T_{AC} = \frac{T_{AB}T_{BC}}{1 - R_{BA}R_{BC}}. \tag{12a, 12b}$$

The complex eigenfrequencies (ω_n) of the system shown in Fig. 4 are obtained by solving the characteristic equation

$$F(\omega) = e^{-i\omega L/c} - R_0 R_{AC} e^{i\omega L/c} = 0. \tag{13}$$

3.2 Green's function approach

We model the thermoacoustic interaction in the tube with a Green's function approach. This requires the tailored Green's function, denoted by $G(x, x', t, t')$, which is the response observed at position x and time t to a point source at position x' firing an impulse at time t'. Naturally, this is a superposition of modes n,

$$G(x, x', t, t') = H(t - t') \sum_{n=1}^{\infty} Re\left[G_n(x, x') e^{-i\omega_n (t - t')}\right], \tag{14}$$

$H(t - t')$ is the Heaviside function (it guarantees causality, i.e. $G = 0$ for $t < t'$); ω_n is the complex eigenfrequency of the tube without flame and given by Eq.(13); G_n is the Green's function amplitude and given by

$$G_n(x, x') = -\frac{c}{2L} R_0 T_{AC}^2 e^{2i\omega_n x_q/c}. \tag{15}$$

The calculations that lead to these results are based on the configuration in Fig. 5, with the impulsive source situated at x'. They are quite lengthy; details can be found in [1].

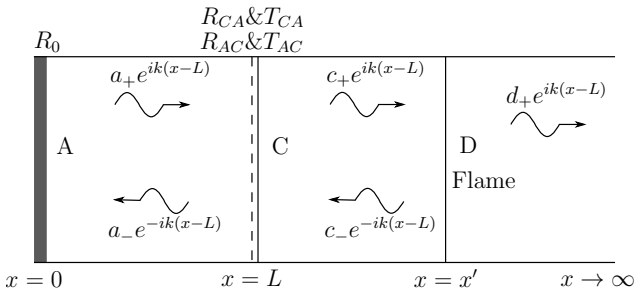

Figure 5: Analytical representation of the burner with a heat source located at $x = x'$.

The tailored Green's function allows one to derive an ODE for the velocity of an individual mode n, driven by a compact flame situated at x_q. Again, the calculations are too long to be shown here; details can be found in [1]. The resulting ODE has the form

$$\ddot{u}' + a_1\dot{u}' + u' = 0, \tag{16}$$

with,

$$a_1 = -2Im(\omega_n) - B\,Im(\omega_n G_n^*)\alpha\left[n_1\int D(\tau-\tau_{c_1})\frac{\sin(\Omega\tau)}{\Omega}d\tau + n_2\int D(\tau-\tau_{c_2})\frac{\sin(\Omega\tau)}{\Omega}d\tau\right] - B\,Re(G_n)\alpha\left[n_1\int D(\tau-\tau_{c_1})\cos(\Omega\tau)d\tau + n_2\int D(\tau-\tau_{c_2})\cos(\Omega\tau)d\tau\right], \tag{17}$$

and

$$a_0 = \left|\omega_n^2\right| + B\,Im(\omega_n G_n^*)\alpha\left[n_1\int D(\tau-\tau_{c_1})\cos(\Omega\tau)d\tau + n_2\int D(\tau-\tau_{c_2})\cos(\Omega\tau)d\tau\right] - B\,Re(G_n)\alpha\left[n_1\int D(\tau-\tau_{c_1})\Omega\sin(\Omega\tau)d\tau + n_2\int D(\tau-\tau_{c_2})\Omega\sin(\Omega\tau)d\tau\right]. \tag{18}$$

The new quantities appearing in these equations are:$B = -(\gamma-1)/c^2$ (abbreviation), $\Omega \approx Re(\omega_n)$, and α (this is a constant factor relating the local heat release rate and the global heat release rate). Clearly, Eq. (16) is the equation for a damped harmonic oscillator. a_1 is the damping coefficient and hence an indicator of the stability behaviour: mode n is stable if $a_1 \geq 0$ and unstable otherwise.

4. Stability Predictions

We made stability predictions for a matrix burner with properties listed in Table 2.

Table 2: Geometry and other parameters of the matrix burner.

Parameter	Value
Tube radius, a	0.035m
Length of the tube, L	0.1 to 0.8 m (variable)
Thickness of the perforated plate, h	0.003m
Number of perforations per unit area, $\mathcal{N}$	1.09×10^5/m^2
Radius of perforations, r_p	0.001m
factor relating local and global heat release rate, α	3×10^5 m^2 s^{-2}
Distance of flame from perforated plate, $x_q - L$	0.01m
Specific heat ratio, γ	1.4
Speed of sound, c	$345m/s$

Two parameters were varied to construct stability maps: The tube length L ranges from $0.1m$ to $0.8m$, and the amplitude $A/\bar{u}$ from 0 to 2. The map for mode *n*=1 is shown in Fig. 6c. The region of instability is marked in grey. It has the shape of a tongue emerging from the bottom left corner and agrees qualitatively with Noiray's results. However, the quantitative agreement is not so good: the tongue covers L values from 0.1 to 0.4 (rather than from 0.1 to 0.25) and $A/\bar{u}$ values from 0 to 1.7 (rather than from 0 to 0.7). In other words, our predictions overestimate the size of the instability region. We will investigate this discrepancy further in a future study.

In order to illustrate the influence of the two time-lags τ_1 and τ_2, we have produced the Figs. 6a and 6b. Figure 6a shows contours for the difference $(0.5T_{eig} - \tau_1)$ and Fig. 6b for the difference $(0.5T_{eig} - \tau_2)$, where T_{eig} is the period of the fundamental mode (the mode under consideration), estimated by considering the burner as a quarter-wave resonator with eigenfrequency $f_{eig} = c/4L$ and corresponding time period $T_{eig} = 1/f_{eig}$. The zero contour lines are superimposed on the stability map in Fig. 6c. From this figure, it can be seen that the unstable region lies close to the zero lines of the $(0.5T_{eig} - \tau_1)$ and $(0.5T_{eig} - \tau_2)$contours.

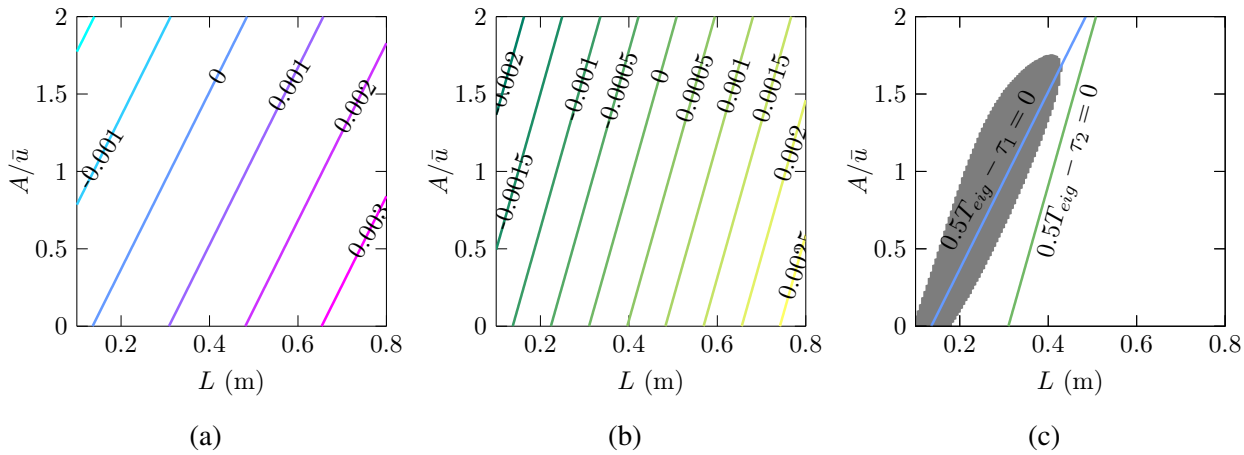

Figure 6: Stability map of a matrix burner using a two time-lag heat release rate law and Green's function approach. (a) Contours of $(0.5T_{eig} - \tau_1)$ (b) Contours of $(0.5T_{eig} - \tau_2)$ (c) Stability map with $(0.5T_{eig} - \tau = 0)$ lines.

5. Summary and outlook

In this paper, we presented a systematic method to approximate a measured FDF by an analytical expression featuring

- several discrete time-lags, τ_1, τ_2, $\cdots$
- Gaussian distributions around each time-lag with standard deviations σ_1, σ_2, $\cdots$
- generalised coupling coefficients n_1, n_2, $\cdots$

Each of these coefficients can be determined by minimising the discrepancy with the experimental FDF data. If this is done for different amplitudes, the amplitude-dependence of the parameters τ_1, τ_2, $\cdots$, σ_1, σ_2, $\cdots$, n_1, n_2, $\cdots$ can be elucidated, and this amplitude-dependence can also be approximated analytically. Altogether, a full analytical description of a measured FDF can be obtained.

We applied this method to a specific laboratory burner (Noiray's matrix burner) and determined the analytical representation of its FDF. We subsequently used this analytical FDF to make stability predictions (based on a Green's function approach) and presented them in the form of a stability map. We obtained good qualitative agreement with Noiray's measured stability map. Also, we observed that the stability map is quite sensitive to the curve fit used to evaluate the amplitude dependence of the model parameters. We used a curve fit which suits the physical behaviour of the matrix flame. Obtaining an optimal fit for the parameters is a part of our work in progress.

6. Acknowledgements

The presented work is part of the Marie Curie Initial Training Network Thermoacoustic and Aeroacoustic Nonlinearities in Green combustors with Orifice structures (TANGO). We gratefully acknowledge the financial support from the European Commission under call FP7-PEOPLE-ITN-2012.

REFERENCES

1. Heckl, M. A. Analytical model of nonlinear thermo-acoustic effects in a matrix burner, *Journal of Sound and Vibration*, **332** (17), 4021–4036, (2013).

2. Heckl, M. A new perspective on the flame describing function of a matrix flame, *International Journal of Spray and Combustion Dynamics*, **7** (2), 91–112, (2015).

3. Noiray, N., Durox, D., Schuller, T. and Candel, S. A unified framework for nonlinear combustion instability analysis based on the flame describing function, *Journal of Fluid Mechanics*, **615**, 139–167, (2008).

4. Noiray, N., *Linear and nonlinear analysis of combustion instabilities, application to multipoint injection systems and control strategies*, Ph.D. thesis, École Centrale Paris, (2007).

5. Gopinathan, S. M., Bigongiari, A. and Heckl, M. A. Time-domain representation of a flame transfer function with generalised $n\tau$ - law featuring a time-lag distribution, *In: Proceedings of the 23rd International Congress on Sound and Vibration*, Athens, Greece, 10–14 July, (2016).

6. Levine, H. and Schwinger, J. On the radiation of sound from an unflanged circular pipe, *Physical Review*, **73**, 383–406, (1948).